Evaluation of the Ordering of Membranes in Multilayer Stacks Built on an ATR-FTIR Germanium Crystal with Atomic Force Microscopy: The Case of the H^+,K^+-ATPase-containing Gastric Tubulovesicle Membranes

Dimitri Ivanov,* Nicolas Dubreuil,* Vincent Raussens,† Jean-Marie Ruysschaert,† and Erik Goormaghtigh†
*Laboratory for Polymer Physics, †Laboratory for the Structure and Function of Biological Membranes, Structural Biology and Bioinformatics Center, Free University of Brussels, Brussels, Belgium

ABSTRACT Polarized attenuated total reflection Fourier transform infrared spectra were recorded on multilayer stacks of native gastric tubulovesicle membranes. The spectral intensity and linear dichroism were measured for average thicknesses ranging between 0 and 100 bilayers. Atomic force microscopy was used to investigate the orientation of the membranes at the top of the stack. Height profiles were obtained along randomly drawn lines and slopes were computed over various distances. Orientation distribution functions were obtained from the slopes and decomposed into Legendre polynomials. It was found that the second Legendre polynomials coefficient characterizing the membrane orientation was always larger than 0.9. It could therefore be concluded that the membrane tilt does not significantly contribute to the infrared dichroism, even for the largest thicknesses tested.

INTRODUCTION

Polarized attenuated total internal reflection (P-ATR) infrared spectroscopy is presently one of the best tools available for the structural study of membrane-embedded peptides and proteins. The method is simple (systems of oriented multilayers are easily obtained by drying a membrane suspension on the internal reflection element), it is sensitive (<1 μg of peptide is required; e.g., Demel et al., 1990), and it does not require specific labeling, although labeling with ^{13}C allows the study of selected residues (Torres et al., 2000, 2001). One of the main interests of P-ATR FTIR spectroscopy is that it yields insight into the orientation of the membrane molecules including protein secondary structures. As such, the method could provide a wealth of information on the organization of protein submolecular domains associated with the membrane. Orientational order parameters can indeed be derived from the dichroic ratio of the protein amide I or amide II bands. Yet, the determination of secondary structure orientation is subject to uncertainties from several origins. For the clarity of the subsequent discussion, we consider below that the orientation of an α-helix long symmetry axis with respect to the internal reflection element (IRE) surface normal is to be determined. The discussion, however, stands in the general case for any transition with uniaxial symmetry. R^{ATR} is the experimental ratio between the absorbance of one band recorded with the incident light polarized parallel to the incidence plane ($A^{\parallel}$) and the absorbance recorded with the perpendicular polarization ($A^{\perp}$):

$$R^{ATR} = \frac{A^{\parallel}}{A^{\perp}}. \quad (1)$$

It is related to the molecular orientation through the order parameter S according to

$$R^{ATR} = \frac{E_x^2}{E_y^2} + \frac{E_z^2}{E_y^2}\left(1 + \frac{3\,S_{experimental}}{1 - S_{experimental}}\right), \quad (2)$$

where E_x^2, E_y^2, and E_z^2 are the time-averaged square electric field amplitudes of the evanescent wave in the film at the IRE/film interface (Goormaghtigh and Ruysschaert, 1990). $S_{experimental}$ contains the information on the mean orientation of the transition dipole and on the distribution of the dipole orientations at their mean value. From FTIR dichroism measurements, only the projection of the angular distribution on the second Legendre polynomials can be measured (Rothschild and Clark, 1979). The latter is simply referred to as the order parameter (S) in the literature. The measured order parameter S, denoted below $S_{experimental}$, is directly obtained from infrared dichroic ratios (Rothschild and Clark, 1979; Fringeli and Günthard, 1981), reviewed in Goormaghtigh and Ruysschaert (1990), assuming an uniaxial symmetry (Rothschild and Clark, 1979; Goormaghtigh and Ruysschaert, 1990; Bechinger et al., 1999).

The measured order parameter S, denoted $S_{experimental}$, obtained from R^{ATR} through Eq. 2 can be generally expressed as the product of several order parameters related

Submitted February 23, 2004, and accepted for publication May 3, 2004.

Address reprint requests to Dr. E. Goormaghtigh, Laboratory of Structure and Function of Biological Membranes, Université Libre de Bruxelles, CP 206/2, Boulevard du Triomphe, B-1050 Brussels, Belgium. Tel.: 32-2-650-5386; Fax: 32-2-650-5382; E-mail: egoor@ulb.ac.be.

Abbreviations used: AFM, atomic force microscopy; ATR, attenuated total reflection; FTIR, Fourier transform infrared; IRE, internal reflection element; P-ATR: polarized attenuated total reflection.

0006-3495/04/08/1307/09 $2.00

doi: 10.1529/biophysj.104.041863

to a set of nested, uniaxial symmetric distributions (Rothschild and Clark, 1979). In this condition,

$$S_{\text{experimental}} = S_{\text{membrane}}\, S_{\text{helix}}\, S_{\text{dipole}}, \quad (3)$$

where S_{membrane} describes the distribution of the lipid membrane patches (smallest planar membrane unit) with respect to the internal reflection element; S_{helix} describes the orientation of the helices within the membrane plane; and S_{dipole} describes the dipole orientation of either amide I or amide II with respect to the helix axis. A schematic representation of these nested distributions appears in Fig. 1. For the sake of the clarity, each contribution to the product (Eq. 3) can be seen itself as the product of the mean tilt contribution, i.e., the angles γ_0, β_0, and α_0 as represented on Fig. 1, by the contribution of the disorder characterized by the distribution of the angular values at their mean.

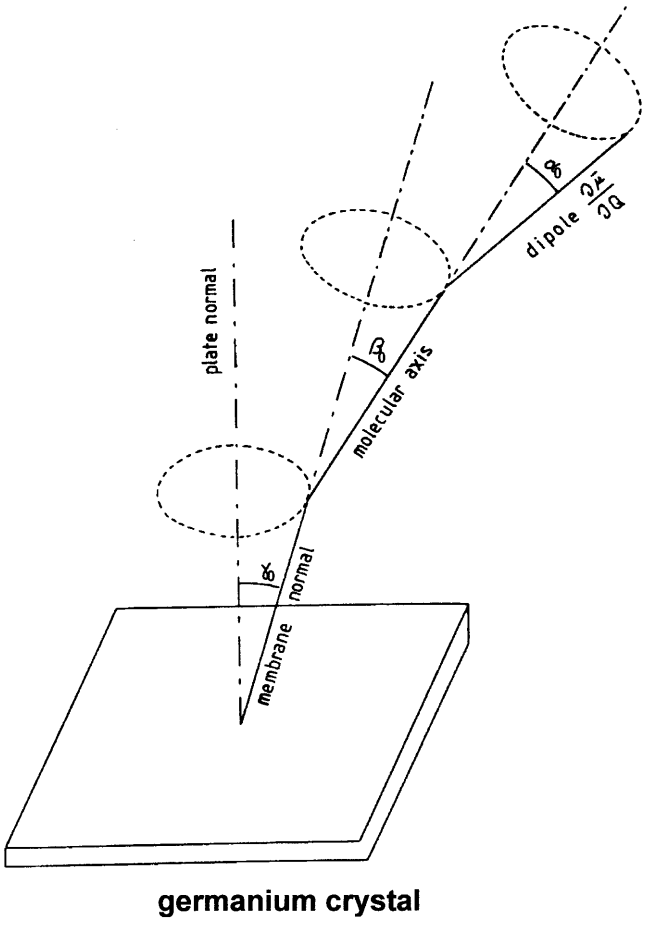

FIGURE 1 Set of nested axially symmetric distributions. The membrane normal is distributed at the germanium crystal normal (angle γ_0), the secondary structure axis at the membrane normal (angle β_0), and the transition dipole moment at the secondary structure axis (angle α_0). In addition to the mean values γ_0, β_0, and α_0, some disordering is possible in real systems. It is characterized by the angular distribution of γ, β, and α at their mean values of γ_0, β_0, and α_0 respectively.

It is usually considered that the transition dipole has a unique distribution of the angle α which characterizes the transition (no disordering). The value S_{dipole} can therefore be calculated as $(3\cos^2\alpha_0-1)/2$ and detailed discussions about the orientation α_0 of the transition dipoles for different secondary structures have appeared (Axelsen et al., 1995; Citra and Axelsen, 1996; Marsh et al., 2000; Marsh, 2000; Pali and Marsh, 2001; Marsh and Pali, 2001). The value S_{helix} can then be evaluated from $S_{\text{experimental}}$ provided that S_{membrane} is known.

The ordering of the membrane on the ATR crystal is usually considered to be ''good'' but only a few publications indicate that S_{membrane} could be close to 1 (Rothschild et al., 1980; Zhang et al., 1995a,b). Polarized ATR spectra were recorded on the sarcoplasmic reticulum Ca^{2+}-ATPase. The anisotropy was found to be the highest in dry films and was found to decrease upon increasing hydration and membrane thickness (Buchet et al., 1991). AFM was used for the first time to characterize the IRE surface in the presence and in the absence of a monomolecular film by Axelsen et al. (1995). On a 512 × 512 datapoint image covering a 2 × 2 μm region of the crystal, Axelsen determined an order parameter of 0.65 and 0.82 for untreated and silanized crystal respectively, suggesting that the acyl-silane chains effectively reduce surface imperfections. Yet, the problem of the ordering in thick membrane stacks remains largely unaddressed.

The case of the gastric ATPase-containing tubulovesicles is of particular interest. These vesicles are recycled from the plasma membrane into intracytoplasmic vesicles as a storage form for the gastric ATPase and can be extracted as such from the stomach apical cells; see Yao and Forte (2003) for a review. The main protein present in the membrane is the gastric H^+,K^+-ATPase, a glycosylated protein responsible for stomach lumen acidification. Importantly, it has been shown before that thick multilayers systems built by simple drying of a tubulovesicle suspension are stable for hours in an aqueous flow, indicating the presence of strong interactions between the membranes. It has also been shown in the same system that the enzyme remains active and fully accessible to ligands that shift its conformation from the E1 to the E2 form of the enzyme (Vander Stricht et al., 2001; Scheirlinckx et al., 2004), indicating that the multilayer stack also presents large aqueous channels in its structure that allow ligands to quickly migrate through an ~100-bilayers-thick stack. Such a case is not unique; membrane stacks containing biotinylated PE were also found to be fully accessible to streptavidin, i.e., a homotetrameric protein (4 × 13 kDa; Acha et al., 2001).

In the present communication we address the issue of the membrane ordering for stacks made out of tubulovesicle membranes of different thicknesses using atomic force microscopy. It is found that membrane ordering remains very good ($S_{\text{membrane}} > 0.9$) up to the thickest stacks considered.

MATERIALS AND METHODS

Materials

Preparation of the tubulovesicles

Tubulovesicles were isolated from hog gastric fundus by differential centrifugation as described previously (Soumarmon et al., 1980). They were further purified from the microsomal fractions by centrifugation on a discontinuous sucrose density gradient at 100,000 *g* overnight. The material collected at the 8–30% sucrose interface is referred to as the tubulovesicles.

Protein assay

Proteins were assayed using the BCA kit from Pierce (Rockland, IL). Bovine serum albumin was used as standard.

ATPase activity

ATPase activity of the tubulovesicles was determined in a medium containing 40 mM HEPES, 2 mM ATP, 2 mM $MgCl_2$ at pH 7.2 in the presence or in the absence of 20 mM KCl. The vesicles were incubated at 37°C for 15 min in this medium. The reaction was stopped by addition of 7% SDS (final concentration 1.75%). Inorganic phosphate formation was assayed according to Stanton (1968) except that the coloration was revealed with ascorbate. Sucrose was 8% (w/v) to keep iso-osmotic conditions. This is necessary to obtain sealed vesicles (Raussens et al., 1997). ATPase activity expressed in μmol h^{-1} per mg^{-1} protein at 37°C is 36 ± 7 and 111 ± 30 after addition of 14 μM nigericin for uncoupling conditions, in line with previously published values.

Techniques

FTIR spectroscopy

Attenuated total reflection infrared (ATR-FTIR) spectra were recorded on a Bruker Equinox 55 infrared spectrometer equipped with a liquid nitrogen cooled mercury-cadmium telluride detector. The internal reflection element (IRE) was a trapezoidal germanium ATR plate (50 × 20 × 2 mm) with an aperture angle of 45° yielding 25 internal reflections (ACM, Villier St. Frederic, France). 256 scans were averaged for each spectrum. Spectra were recorded at a nominal resolution of 2 cm^{-1}. The spectrometer was continuously purged with air dried on a FTIR purge gas generator 75–62 Balston (Maidstone, England) at a flow rate of 10 l/min. Spectra were recorded with incident light polarized parallel or perpendicular relative to the incidence plane.

Atomic force microscopy

Atomic force microscopy (AFM) images were obtained using a multimode atomic force microscope coupled with a Nanoscope III controller (Digital Instruments, Santa Barbara, CA). The multimode atomic force microscope was equipped with an E-scanner. Samples were imaged in tapping mode with a rectangular silicon cantilever (Nanosensors, type NCH) in ambient conditions. Topographic, phase, and amplitude data were collected. The integral and proportional gains and the scan rate were optimized for providing the best correspondence between line trace and retrace. AFM data were not filtered, although the topographic image data were background-corrected to eliminate the sample tilt. The treatment of images and cross-section analysis were performed with a home-made software (Basire and Ivanov, 2000). Four different image sizes were used: 15 × 15 μm^2 (1 datapoint every 38 nm), 5 × 5 μm^2 (1 datapoint every 12 nm), 1 × 1 μm^2 (1 datapoint every 2.5 nm), and 500 × 500 nm^2 (1 datapoint every 1 nm).

Sample preparation

The germanium IRE were cleaned just before use sequentially with a lab detergent (Decontamin 11, SA InterSciences, Brussels, Belgium), distilled water, methanol, and chloroform. They were then placed in a plasma cleaner PDC-23G (Harrick, 1967) for 5 min. For ATR-FTIR, thin films were obtained as described by Fringeli and Günthard (1981) by slowly evaporating the tubulovesicles under a N_2 stream on one side of a germanium IRE. The covered area was close to 3 cm^2. Concentrations (lipid + protein) were computed assuming a protein/lipid ratio (w/w) of 1.2. Concentrations were adjusted to spread volumes between 5 and 15 μl over 3 cm^2. For AFM imaging, 1-cm^2 Ge crystal plates were cut from an ATR germanium trapezoidal plate with a diamond saw.

Analysis

$\langle P_2 \rangle$ computation

The dichroic ratio R^{ATR} (Eqs. 1 and 2) does not only depend on the mean orientation of the transition dipole but also on the distribution of the values around the mean (Eq. 3). The orientation of the membranes with respect to the germanium surface can be characterized on the one hand by the mean value of their tilt with respect to the germanium surface and, on the other hand, by the disordering around this mean value. The latter is characterized by the shape of the distribution of the angular values at the mean. The mean membrane orientation is found here to be parallel to the germanium surface. This is in agreement with a uniaxial symmetry axis perpendicular to the surface of the germanium crystal and with the mode of preparation of the samples. Because of the geometry of the ATR experiment, the simplest and most efficient way to describe the distribution of the orientations is in terms of Legendre polynomials. In general, any distribution of the membrane patch tilts $D(\theta)$ can be described using a series of Legendre polynomials $P_n(\cos\theta)$ (Rothschild and Clark, 1979; Goormaghtigh and Ruysschaert, 1990),

$$D(\theta) = \sum_{n=0}^{\infty} \frac{2n+1}{2} \langle P_n \rangle P_n(\cos\theta), \tag{4}$$

where the $\langle P_n \rangle$ values are the coefficients determined from the experimentally obtained orientation distribution. The odd terms of P_n are zero because of the symmetry with respect to the membrane plane (Rothschild and Clark, 1979). The first two even-order Legendre polynomials are given by

$$P_0(\cos\theta) = 1;$$
$$P_2(\cos\theta) = \frac{3\cos^2\theta - 1}{2}. \tag{5}$$

Remarkably, because of the symmetry of the experiment, it can be demonstrated that only these two Legendre polynomials contribute to the IR dichroism (Rothschild and Clark, 1979; Goormaghtigh and Ruysschaert, 1990). The coefficient $\langle P_n \rangle$ can be evaluated as

$$\langle P_n \rangle = \frac{\int_0^{\frac{\pi}{2}} D(\theta) P_n(\cos\theta) \sin\theta \, d\theta}{\int_0^{\frac{\pi}{2}} D(\theta) \sin\theta \, d\theta}. \tag{6}$$

It means that whatever the shape, $D(\theta)$, of the distribution of the tilts at the mean value θ_0, the $\langle P_0 \rangle$ and $\langle P_2 \rangle$ coefficients fully describe the IR dichroism even if they probably poorly describe the bell-shaped angular distribution. The value of the coefficient $\langle P_2 \rangle$ is usually called ''order parameter,'' S, as it describes the disordering around the mean value for P-ATR experiments. In the present work, $D(\theta)$ for the membranes is directly measured from AFM images and its projection on P_2, i.e., $\langle P_2 \rangle = S_{membrane}$, evaluated according to Eq. 6.

RESULTS AND DISCUSSION

In the experiments below, increasing amounts of tubulovesicles (lipid + protein, 0.47 μg, 0.94 μg, 1.88 μg, 4.7 μg, 9.87 μg, and 47 μg per cm^2) were spread and dried under an N_2 flow on an ATR germanium crystal, yielding an average number of lipid bilayers of 1, 2, 4, 10, 20, and 100, respectively, for the multilayer stack. For this computation, we assumed a lipid molecular weight of 750, an area per lipid molecule of 60 Å^2, a protein/lipid ratio of 1.2, and 50% of the area occupied by the lipids. This rough approximation is solely intended to give an estimate of the film thickness and is in no way used for any quantitative determination in the present work.

Atomic force microscopy

Images were recorded over 15 × 15 μm^2, 5 × 5 μm^2, 1 × 1 μm^2, and 0.5 × 0.5 μm^2. Typical amplitude and phase images are presented in Fig. 2 for 0, 0.47, and 4.7μg/cm^2 of tubulovesicle materials. Clearly, the clean germanium plate provided by the manufacturer presents grooves resulting from the polishing. Measurements at higher magnification indicate that the largest grooves are ~50-nm wide (not shown). It must be noted that this is much smaller than the IR wave amplitude (2–5 μm in the range of interest for membrane studies). Remarkably, addition of tubulovesicle membranes in a small amount (approximately just enough to cover the area) smears out the amplitude image while the grooves resulting from the polishing can still be detected in the phase image. This result demonstrates that when small amounts of membranes are spread on the germanium area, a rather homogenous film is formed. Further addition of membrane materials fully hides these grooves.

Height profiles and height distributions

Height profiles were measured along lines arbitrarily drawn through the images. Two examples of such profiles are reported in Fig. 3 for the clean germanium surface and that containing 0.47 μg of tubulovesicles. The ''smoothing'' effect of the first bilayer is evident from the profiles reported in Fig. 3. The height distributions obtained directly from the height profiles are reported in Fig. 4. It may be observed that among the examples reported in Fig. 4, some samples seem to present discrete height populations that might correspond to the addition of an integer number of bilayers of ~15–20 nm each. Fourier transform of several height distributions (but not all) revealed a periodicity ~1/15–1/20 nm^{-1}, a reasonable estimate for the overall thickness of the tubulovesicle membranes (not shown). This value is in agreement with the size of the sarcoplasmic Ca^{2+}-ATPase, 14 nm (Toyoshima et al., 2000). The fact that steps are detected in height profiles and approximately correspond to a bilayer thickness indicates that the slopes reported below could be overestimated because these steps were considered as a membrane tilt.

Slope distribution

Slope distributions were obtained from the height cross-sections such as those presented in Fig. 3. Local slopes were computed over different distances D ranging between 1 and 200 nm to investigate the scale dependence of the roughness

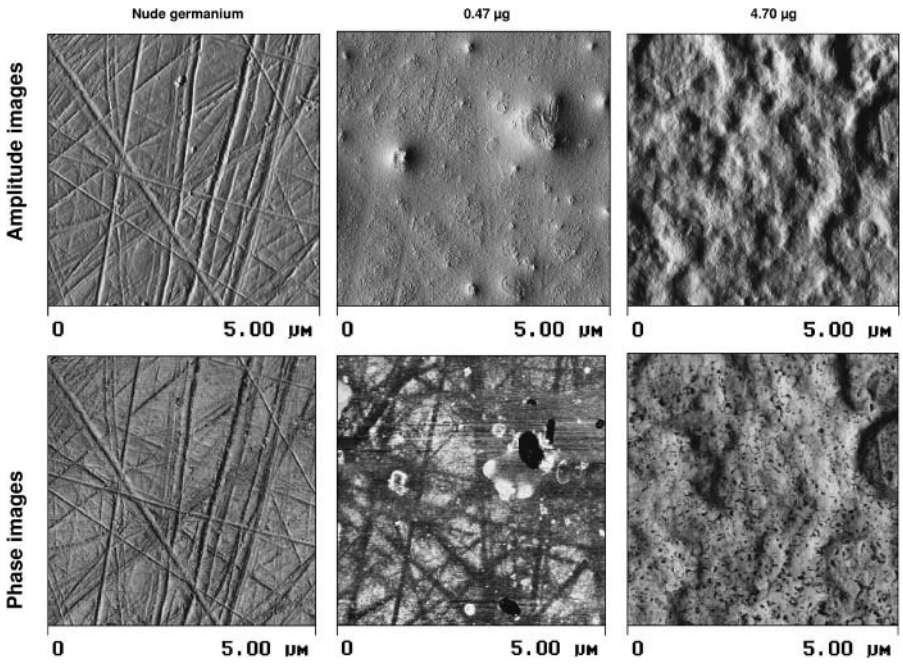

FIGURE 2 Amplitude and phase images of a 5 × 5 μm^2 of ATR nude germanium or germanium covered with 0.47 or 4.7 μg of tubulovesicle materials on a 1-cm^2 ATR germanium crystal cut out of the trapezoidal plate used for FTIR experiments.

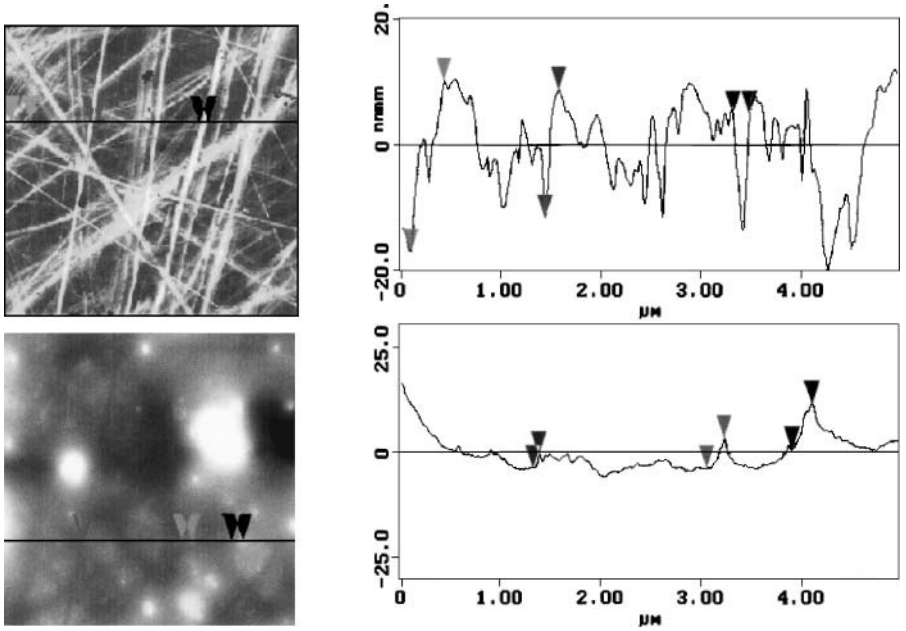

FIGURE 3 Representative height profiles obtained along a line through the AFM image (height image, $5 \times 5\ \mu m^2$). The arrows on the image (*left*) are reported on the height profile (*right*). A clean germanium crystal surface was used (*top*) and a crystal covered with 0.47 μg of tubulovesicles/cm^2 (*bottom*). The latter amount corresponds to an average of approximately one bilayer present on the area.

of the surface. The effect of the distance D over which the slope is computed is discussed below. The slopes were evaluated from the tangents of the linear fit for all the datapoints between two points i and $i + NP-1$ (NP = number of datapoints over the distance D) for all the points i in the height profile. Slopes were converted in degrees and the slope distribution functions were then established from all the slopes obtained. Examples of slope distributions are reported in Fig. 5.

Evaluation of $\langle P_2 \rangle$

The value of $\langle P_2 \rangle$ was computed for all the profiles and images obtained in the course of this study (Eq. 6). At this stage, it was necessary to decide on which scale the slope must be evaluated. The slope to be considered in this work is the slope which characterizes the general lipid bilayer orientation but not the individual phospholipid molecules. Membrane-embedded protein orientation must, in polarized ATR-FTIR experiments, be defined with respect to the general membrane orientation to decide whether the tilt measured origins from the tilt of the protein secondary structure with respect to the membrane, or from the tilt of the membrane itself with respect to the germanium support. In turn, relevant slopes should be evaluated on a distance D slightly longer than the molecular size. A phospholipid molecule has a diameter $\approx$0.85 nm. A membrane-embedded protein has a much larger diameter (the diameter of the gastric ATPase, which is, by far the dominant protein in these membranes, is $\sim$4–5 nm). We tested several distances (1, 2, 5, 20, 50, and 200 nm) to compute the slopes. The resulting $\langle P_2 \rangle$ obtained for different image sizes and resolutions are reported in Fig. 6 as a function of the distance D. It appears from Fig. 6 that the order parameter is always $>$0.95 with only a small increase upon increasing the distance over which the slope is computed. It turns out that the distance D and the image resolution have little effect on the value of $\langle P_2 \rangle$.

Dependence on the film thickness

The effect of film thickness on the $\langle P_2 \rangle$ is reported in Fig. 7 for tubulovesicle amounts varying between 0 and 47 μg spread over the 1-cm^2 area. The slopes were computed over a distance of 2 nm. It appears that $\langle P_2 \rangle$ is always $>$0.9, even for the largest amount tested.

Infrared spectroscopy

For FTIR experiments, an area of 3 cm^2 was covered by the membrane film. Spectra recorded for increasing amount of materials are shown in Fig. 8. The lipid band found between 1762 and 1705 cm^{-1} can be safely assigned to the lipid ester ν(C=O). Globally the dichroism of this band is close to zero and can be used as a good approximation of a magic-angle transition dichroism (Bechinger et al., 1999; Goormaghtigh et al., 1999). A major contribution of the lipids also appears at 1468 cm^{-1} and can be assigned to $\delta(CH_2)$. Two important protein bands are found in the spectral window that exists in the phospholipid spectrum between 1700 and 1500 cm^{-1}. Amide I (1700–1600 cm^{-1}) is the most intense absorption band of the polypeptides. Amide ν(C=O) has a predominant role in amide I, accounting for 70–85% of the potential energy. ν(C-N) follows with 10–20% of the potential energy and the C-CN deformation may account for $\sim$10% of the potential energy (Krimm and Bandekar, 1986). Amide I also

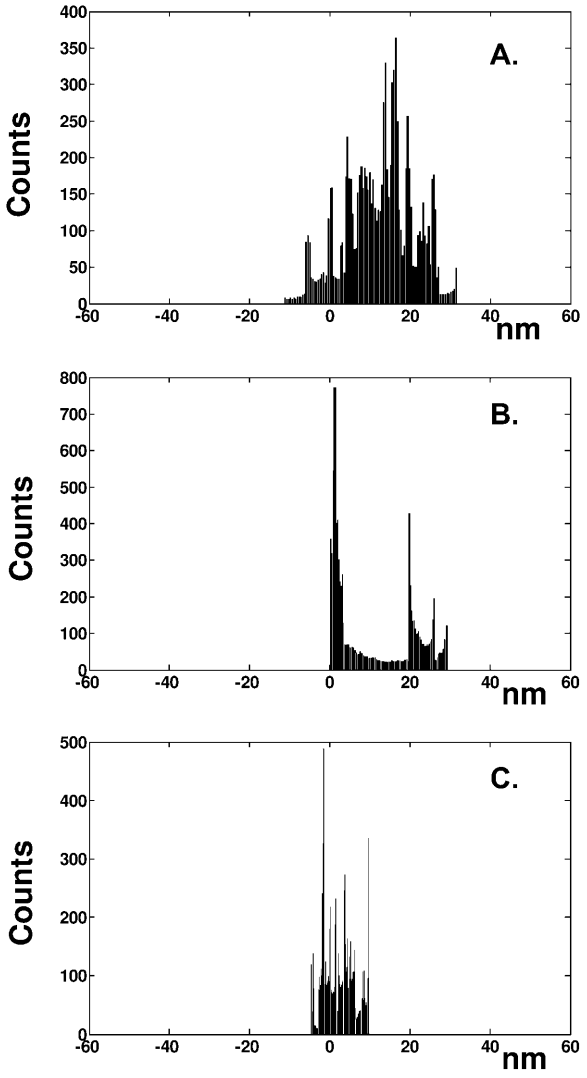

FIGURE 4 Height distributions obtained on $5 \times 5\ \mu m^2$ images for 0 (*A*), 0.47 (*B*), and 47 (*C*) μg of tubulovesicles/cm^2. The location of zero height is arbitrary.

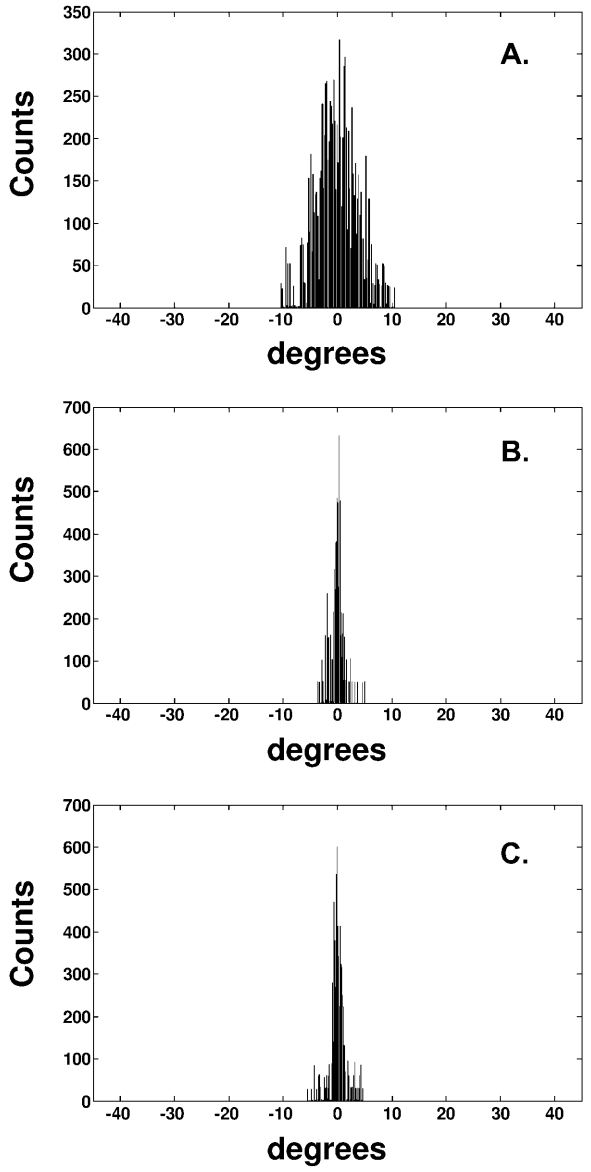

FIGURE 5 Slope distributions obtained on $5 \times 5\ \mu m^2$ images for 0 (*A*), 0.47 (*B*), and 47 (*C*) μg of tubulovesicles/cm^2.

contains some in-plane NH bending contribution which is mainly responsible for the downshifts in the amide I frequency on N-deuteration (Krimm and Bandekar, 1986). Amide I shape is conformationally sensitive and generally used for secondary structure determination (for reviews, see Goormaghtigh et al., 1994a,b; Arrondo and Goni, 1999). The evolution of the integrated intensity of amide I, amide II, and $\nu_{\text{lipid ester}}$C=O as a function of the amount of membranes spread over the given crystal area appears in Fig. 9. As a first approximation, the spectral intensity increases as $k(1-e^{-2z/dp})$ (Fringeli, 1992) where z is the film thickness from the germanium interface, k is a constant that depends on the extinction coefficient and dp is the penetration depth, i.e., the depth at which the electric field intensity falls to $1/e$ of its value at the interface (see Goormaghtigh et al., 1999 for a review). Using a membrane thickness of 15 nm (as mentioned earlier, this value is in agreement with the size of the sarcoplasmic Ca^{2+}-ATPase, 14 nm—Toyoshima et al., 2000—and with the AFM data above) to evaluate the total S_{membrane} stack thickness, curve-fitting with $k(1-e^{-2z/dp})$ (Fig. 9) for the ester ν(C=O), amide I, and amide II, yields $dp = 0.298$, 0.267, and 0.273 μm, respectively. This demonstrates the consistency of the measurements, and is in no bad agreement with the theoretical value of 0.378 μm at 1730 cm^{-1}, considering the refractive indices of 4.0, 1.44, and 1.0 for germanium, the membranes, and air, respectively (see Goormaghtigh et al., 1994a). Fig. 10 indicates that the dichroic ratio, i.e., the ratio $A^{\parallel}/A^{\perp}$, also depends on the film thickness. This is due to the well known difference in the penetration depth of the parallel and perpendicular polarizations and has been described in detail before (Harrick,

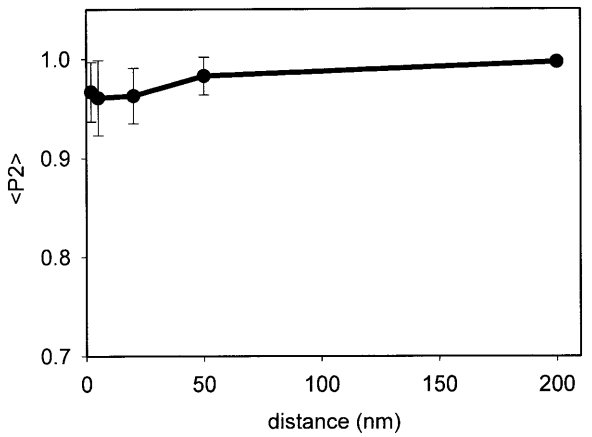

FIGURE 6 Evolution of $\langle P_2 \rangle$ as a function of the distance over which the slope is computed (see text). The amount of tubulovesicle material is 4.7 μg.

1967). Fig. 10 indicates that converting the measured dichroic ratios in $S_{\text{experimental}}$ (Eq. 2) requires the knowledge of the film thickness. It has been suggested earlier that the lipid ν(C=O) can be used to retrieve the apparent film thickness (Bechinger et al., 1999) which fully explains the lipid ν(C=O) dichroism evolution with the amount of materials present in the film. Furthermore, this apparent thickness includes any lack of accuracy on the refractive indices (Bechinger et al., 1999). It must be stressed here that the ester ν(C=O) dichroic ratio should reach a theoretical value of 2 for infinite thickness (see Eq. 36 in Goormaghtigh et al., 1999). With only 100 bilayers, the data presented on Fig. 10 do not reach this limit value.

We can now attempt to evaluate the average helix tilt in the membrane. It can be assumed that the gastric H^+,K^+-ATPase is the most representative protein present in the tubulovesicle membranes (~85%). Assuming also that only the transmembrane segments (10 transmembrane helices for the α-subunit and 1 for the β-subunit) have a net orientation among the 1324 amino-acid-residue-long protein and assuming an average length of 20 residues per

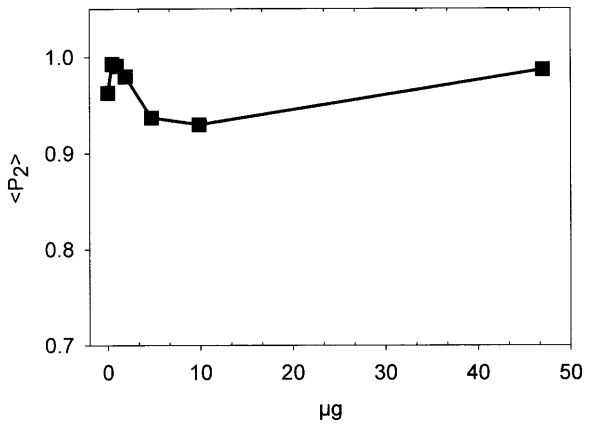

FIGURE 7 Evolution of $\langle P_2 \rangle$ as a function of the amount of tubulovesicle materials spread/cm^2. A distance of 2 nm was used to compute the slopes (see text). The standard deviation ($n = 6$) is included in the symbols.

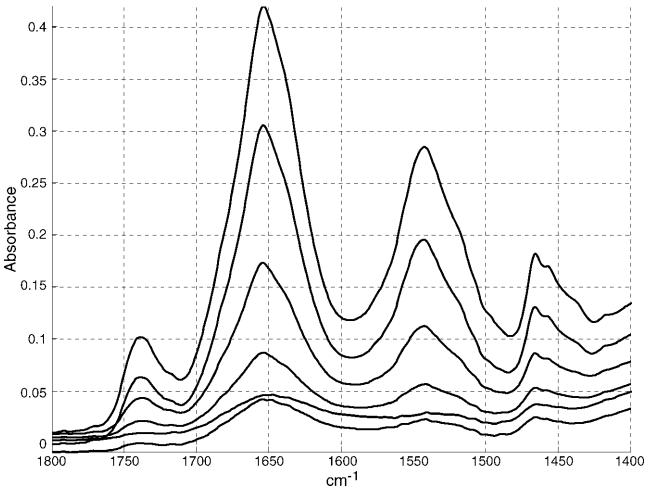

FIGURE 8 Series of ATR-FTIR spectra of tubulovesicles. The amount of materials was 1.4, 2.8, 5.6, 14, 30, and 141 μg (from *bottom* to *top*) spread over an area of 3 cm^2.

transmembrane segment, it turns out that ~16% of the polypeptide chain would contribute to the dichroism. As demonstrated earlier, in such a case (Raussens et al., 1997) the dichroic ratio of the oriented helices R^α is given by

$$R^\alpha = A_\alpha^{90^\circ}/A_\alpha^{0^\circ} = \frac{R - \dfrac{R+2}{2R^{\text{iso}}+1}(1-x)}{1 - \dfrac{1}{R^{\text{iso}}}\dfrac{R+2}{2R^{\text{iso}}+1}(1-x)}, \qquad (7)$$

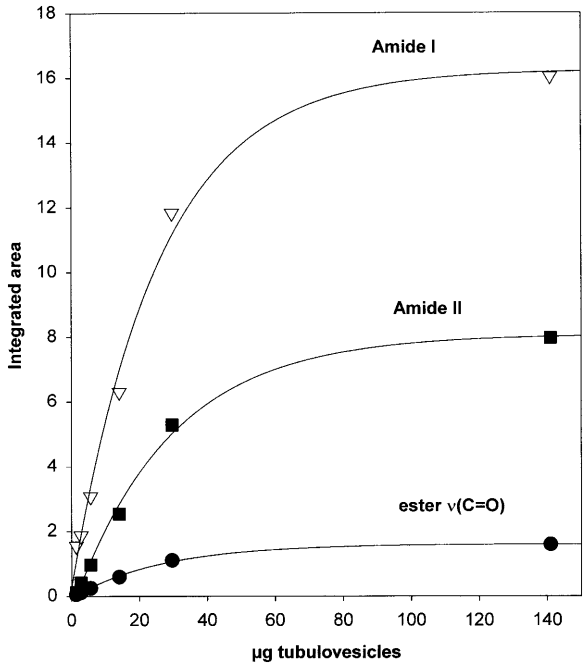

FIGURE 9 Evolution of the integrated area of the amide I (1705–1595 cm^{-1}), amide II (1595–1485 cm^{-1}), and lipid ν(C=O) (1765–1711 cm^{-1}) as a function of the amount of tubulovesicles; see Fig. 8 for the experimental conditions.

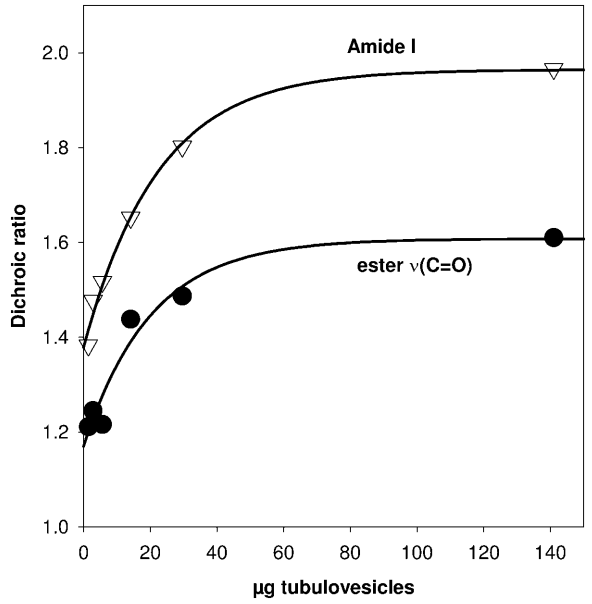

FIGURE 10 Evolution of the dichroic ratio of the amide I and lipid ν(C=O) bands as a function of the amount of materials spread on the germanium crystal. The dichroic ratio is evaluated as the ratio of the integrated area obtained on spectra recorded with parallel and perpendicular polarizations.

where R^{iso} is the dichroic ratio of an unordered contribution and x is the fraction of the ordered contribution (16% here). The different contributions to the order parameter can now be evaluated according to Eq. 3. $S_{experimental}$ is obtained from R^{α} as described earlier (Rothschild and Clark, 1979; Fringeli and Günthard, 1981; Goormaghtigh and Ruysschaert, 1990). The tilt of the dipole with respect to the helix axis has been evaluated to be $\sim$38° for the α-helix (Marsh et al., 2000). S_{dipole} can be evaluated as $(3\cos^2(38°)-1)/2 = 0.43$. The present work indicates that we can confidently assign a value of 0.9 for $S_{membrane}$. S_{helix} can now be calculated. S_{helix} was calculated for all the thicknesses investigated here, taking into account the apparent film thickness derived from the lipid ν(C=O) as described earlier (Bechinger et al., 1999). Its values range between 0.55 and 0.71, corresponding to an average tilt between 26° and 33° for the helix axis with respect to the membrane normal. These values are in close agreement with the recently obtained structure of another P-type ATPase (Toyoshima et al., 2000; Toyoshima and Nomura, 2002).

DISCUSSION

The approach we have followed implies a number of assumptions. Because only the upper layer can be examined with the AFM, we implicitly assumed that the tilts obtained at low membrane concentration remain unchanged as additional material was added on its top. This assumption is important since the contribution to the infrared spectrum of the layers that are close to the germanium crystal is the most important. Even though it would be difficult to understand how a well-oriented layer would form on a disordered support, we could not investigate the lower layer orientations when additional material was present above them. An additional assumption we made is that the uniaxial symmetry depicted in Fig. 1 for the orientation of the membranes is correct. Since the vesicles were dried without stretching or shearing forces applied, any other type of symmetry seems to be very unlikely. Furthermore, we examined a large number of images over different distances from 1 to 20 μm and we examined the height profiles in all directions without being able to point out differences in the height profiles correlated with the direction of the analysis.

The microscopic nature of the slopes reported in Fig. 5 must also be discussed. Fig. 4 suggests that discrete steps are present at the surface of the membrane stacks. As already mentioned, such steps have been unduly considered here as contributing to the tilt of the membranes. It turns out that including the effect of these steps in the overall tilt of the membranes can only result in an underestimate $S_{membrane}$.

It must also be stressed here that the mean slopes computed under the assumption that the cross-sections are traced at random angles are different from the dihedral angles characterizing the tilt of the membranes with respect to the supporting germanium surface. This effect potentially overestimates the value of $S_{membrane}$. The relation between this dihedral angle and the mean angle obtained from the experimental measurements was computed (not shown). It was found that within the range of values discussed in this article, the mean angle obtained experimentally is a good approximation of the dihedral angle (maximum difference $<$10°). When evaluated in terms of $\langle P_2 \rangle$, the overestimation for a Gaussian distribution with a full width at half-height of 20° is 0.36. We consider that this error is acceptable in view of the overall accuracy of the FTIR measurements.

The finding that a rather homogenous film is formed upon drying the vesicle suspension on the germanium crystal (Figs. 2 and 3) is important because both spectral intensity and dichroism depend on film thickness. In turn, the coexistence of clusters of materials at some specific spots with empty spaces around would yield different dichroism results and would be essentially useless for quantitative evaluation of protein secondary structure orientations.

Importantly, Fig. 4 also demonstrates that a structural reorganization occurs, from a vesicular state to a planar system as demonstrated for pure lipid vesicles elsewhere (Johnson et al., 2002).

This work was funded by a grant from the Action de Recherches Concertées, Communauté Française de Belgique. Dr. Goormaghtigh is Research Director and Dr. Raussens is Research Associate of the Belgian National Fund For Scientific Research.

REFERENCES

Acha, V., J. M. Ruysschaert, and E. Goormaghtigh. 2001. Stacks of close to 100 phospholipid bilayers fully accessible to proteins—an ATR-FTIR-based chemometric analysis on hydrated phospholipid films. *Anal. Chim. Acta.* 435:215–226.

Arrondo, J. L. R., and F. M. Goni. 1999. Structure and dynamics of membrane proteins as studied by infrared spectroscopy. *Progr. Biophys. Mol. Biol.* 72:367–405.

Axelsen, P. H., B. K. Kaufman, R. N. McElhaney, and R. N. Lewis. 1995. The infrared dichroism of transmembrane helical polypeptides. *Biophys. J.* 69:2770–2781.

Basire, C., and D. Ivanov. 2000. Evolution of the lamellar structure during crystallization of a semicrystalline-amorphous polymer blend: time-resolved hot-stage SPM study. *Phys. Rev. Lett.* 85:5587–5590.

Bechinger, B., J. M. Ruysschaert, and E. Goormaghtigh. 1999. Membrane helix orientation from linear dichroism of infrared attenuated total reflection spectra. *Biophys. J.* 76:552–563.

Buchet, R., S. Varga, N. W. Seidler, E. Molnar, and A. Martonosi. 1991. Polarized infrared attenuated total reflectance spectroscopy of the Ca^{2+}-ATPase of sarcoplasmic reticulum. *Biochim. Biophys. Acta.* 1068: 201–216.

Citra, M. J., and P. H. Axelsen. 1996. Determination of molecular order in supported lipid membranes by internal reflection Fourier transform infrared spectroscopy. *Biophys. J.* 71:1796–1805.

Demel, R. A., E. Goormaghtigh, and B. de Kruijff. 1990. Lipid and peptide specificities in signal peptide-lipid interactions in model membranes. *Biochim. Biophys. Acta.* 1027:155–162.

Fringeli, U. P. 1992. In situ infrared attenuated total reflection (IR ATR) spectroscopy: a complementary analytical tool for drug design and drug delivery. *Chimia.* 46:200–214.

Fringeli, U. P., and H. H. Günthard. 1981. Infrared membrane spectroscopy. *Mol. Biol. Biochem. Biophys.* 31:270–332.

Goormaghtigh, E., V. Cabiaux, and J. M. Ruysschaert. 1994a. Determination of soluble and membrane protein structure by Fourier transform infrared spectroscopy. I. Assignments and model compounds. *Subcell. Biochem.* 23:329–362.

Goormaghtigh, E., V. Cabiaux, and J. M. Ruysschaert. 1994b. Determination of soluble and membrane protein structure by Fourier transform infrared spectroscopy. III. Secondary structures. *Subcell. Biochem.* 23:405–450.

Goormaghtigh, E., V. Raussens, and J. M. Ruysschaert. 1999. Attenuated total reflection infrared spectroscopy of proteins and lipids in biological membranes. *Biochim. Biophys. Acta.* 1422:105–185.

Goormaghtigh, E., and J. M. Ruysschaert. 1990. Polarized attenuated total reflection infrared spectroscopy as a tool to investigate the conformation and orientation of membrane components. *In* Molecular Description of Biological Membrane Components by Computer-Aided Conformational Analysis. R. Brasseur, editor. CRC Press, Boca Raton, FL. 285–329.

Harrick, N. J. 1967. Internal Reflection Spectroscopy. Interscience Publishers, New York.

Johnson, J. M., T. Ha, S. Chu, and S. G. Boxer. 2002. Early steps of supported bilayer formation probed by single vesicle fluorescence assays. *Biophys. J.* 83:3371–3379.

Krimm, S., and J. Bandekar. 1986. Vibrational spectroscopy and conformation of peptides, polypeptides and proteins. *Adv. Prot. Chem.* 38:181–364.

Marsh, D. 2000. Infrared dichroism of twisted β-sheet barrels. The structure of *E. coli* outer membrane proteins. *J. Mol. Biol.* 297:803–808.

Marsh, D., M. Muller, and F. J. Schmitt. 2000. Orientation of the infrared transition moments for an α-helix. *Biophys. J.* 78:2499–2510.

Marsh, D., and T. Pali. 2001. Infrared dichroism from the x-ray structure of bacteriorhodopsin. *Biophys. J.* 80:305–312.

Pali, T., and D. Marsh. 2001. Tilt, twist, and coiling in β-barrel membrane proteins: relation to infrared dichroism. *Biophys. J.* 80:2789–2797.

Raussens, V., J. M. Ruysschaert, and E. Goormaghtigh. 1997. Fourier transform infrared spectroscopy study of the secondary structure of the gastric H+,K+-ATPase and of its membrane-associated proteolytic peptides. *J. Biol. Chem.* 272:262–270.

Rothschild, K. J., and N. A. Clark. 1979. Polarized infrared spectroscopy of oriented purple membrane. *Biophys. J.* 25:473–487.

Rothschild, K. J., R. Sanches, T. L. Hsiao, and N. A. Clark. 1980. A spectroscopic study of rhodopsin α-helix orientation. *Biophys. J.* 31: 53–64.

Scheirlinckx, F., V. Raussens, J. M. Ruysschaert, and E. Goormaghtigh. 2004. Conformational changes in the gastric H^+,K^+-ATPase monitored by difference FTIR spectroscopy and hydrogen deuterium exchange. *Biochem. J.* In press.

Soumarmon, A., M. Abastado, S. Bonfils, and M. J. Lewin. 1980. C1-transport in gastric microsomes. An ATP-dependent influx sensitive to membrane potential and to protein kinase inhibitor. *J. Biol. Chem.* 255:11682–11687.

Stanton, M. G. 1968. Colorimetric determination of inorganic phosphate in the presence of biological material and adenosine triphosphate. *Anal. Biochem.* 22:27–34.

Torres, J., P. D. Adams, and I. T. Arkin. 2000. Use of a new label, (13)C=(18)O, in the determination of a structural model of phospholamban in a lipid bilayer. Spatial restraints resolve the ambiguity arising from interpretations of mutagenesis data. *J. Mol. Biol.* 300:677–685.

Torres, J., A. Kukol, J. M. Goodman, and I. T. Arkin. 2001. Site-specific examination of secondary structure and orientation determination in membrane proteins: the peptidic $^{13}C=^{18}O$ group as a novel infrared probe. *Biopolymers.* 59:396–401.

Toyoshima, C., M. Nakasako, H. Nomura, and H. Ogawa. 2000. Crystal structure of the calcium pump of sarcoplasmic reticulum at 2.6 Å resolution. *Nature.* 405:647–655.

Toyoshima, C., and H. Nomura. 2002. Structural changes in the calcium pump accompanying the dissociation of calcium. *Nature.* 418:605–611.

VanderStricht, D., V. Raussens, K. A. Oberg, J. M. Ruysschaert, and E. Goormaghtigh. 2001. Difference between the E1 and E2 conformations of gastric H^+/K^+-ATPase in a multilamellar lipid film system—characterization by fluorescence and ATR-FTIR spectroscopy under a continuous buffer flow. *Eur. J. Biochem.* 268:2873–2880.

Yao, X. B., and J. G. Forte. 2003. Cell biology of acid secretion by the parietal cell. *Annu. Rev. Physiol.* 65:103–131.

Zhang, Y. P., R. N. Lewis, G. D. Henry, B. D. Sykes, R. S. Hodges, and R. N. McElhaney. 1995a. Peptide models of helical hydrophobic transmembrane segments of membrane proteins. 1. Studies of the conformation, intrabilayer orientation, and amide hydrogen exchangeability of Ac-K2-(LA)12- K2-amide. *Biochemistry.* 34:2348–2361.

Zhang, Y. P., R. N. Lewis, R. S. Hodges, and R. N. McElhaney. 1995b. Peptide models of helical hydrophobic transmembrane segments of membrane proteins. 2. Differential scanning calorimetric and FTIR spectroscopic studies of the interaction of Ac-K2-(LA)12–K2-amide with phosphatidylcholine bilayers. *Biochemistry.* 34:2362–2371.